FIELD DISTRIBUTION IN THE INPUT COUPLING REGION OF PLANAR SINGLE-MODE WAVEGUIDES

Werner Klaus [(1)], Walter Leeb [(2)]

[(1)]*National Institute of Information and Communications Technology (NICT),4-2-1, Nukui-Kitamachi, Koganei,Tokyo,184-8795, Email: klaus@nict.go.jp*
[(2)]*Institute of Communications and Radio-Frequency Engineering, Vienna University of Technology, Gusshausstrasse 25/389, A-1040 Wien, Austria, Email: walter.leeb@tuwien.ac.at*

ABSTRACT

We apply a numerical method for calculating the field distribution in the region immediately behind the input facet of a dielectric step-index single-mode slab waveguide. The input waves considered are focused plane waves and Gaussian beams of various diameters, with and without misalignment. The figures obtained show the formation of radiation modes and the development of the fundamental guided mode and thus give hints on how to design pieces of single-mode fibers that are to be used as modal filters, e.g., in astronomical interferometers with excessive nulling requirements.

1. INTRODUCTION

Optical single-mode waveguides constitute a key device in instruments for astronomical interferometry aiming at the investigation of extra-solar planets. To give an example: In ESA's DARWIN mission, the optical fields collected by telescopes will be propagated through a piece of single-mode fiber. Only then they will exhibit the highly identical amplitude distribution and phase distribution required for destructive interference of the (unwanted) radiation originating from the star whose planet is under investigation. Propagating the light through an ideal single-mode waveguide achieves just this. One attempt to analytically estimate the minimum length (as required to achieve proper background suppression by modal filtering) of an otherwise ideal fiber waveguide is found in [1]. This approach, however, could not take into account many of the real-world aspects occurring in fibers.

Here we demonstrate the usefulness of a numerical method in calculating – and visualizing – the distribution of the optical field in the input coupling region of a single-mode waveguide. Examining a 2-dimensional single-mode waveguide in a first step already gives an excellent insight into the power flow immediately after the input facet, shows how a steady state intensity distribution in the vicinity of the core is eventually reached, and also yields the coupling efficiency into the waveguides' fundamental mode. Eventually this method will allow taking into account a non-perfect core-cladding geometry, a finite cladding thickness, an absorbing coating, an input taper, etc. After explaining the system model in Sect. 2 we shortly describe the numerical method applied (Sect. 3) before presenting results for cases where the input radiation is either a focused plane wave (Sect. 4) or a focused Gaussian beam (Sect. 5). We visualize the power flow, show how the fundamental mode develops, and obtain the coupling efficiency as a by-product. Section 6 summarizes the findings.

2. SYSTEM MODEL

Fig. 1 shows the system model used. The step-index slab waveguide consists of a core of thickness 2d (index of refraction n_1) and a cladding with index n_2. A slit of width *A* may be positioned just before the input facet. The incident radiation is focused by a lens, the angle ε and the transverse displacement Δx cover the major misalignments. With z and x we denote the coordinate along which the guided wave is propagating and the transverse direction. For all numerical calculation we took $2d = 4.5\,\lambda$ (λ...wavelength), $n_1 = 1.50375$ and $n_2 = 1.5000$. The relative index difference is thus $\Delta = 0.25\%$, and the normalized frequency is $V = 1.5004$, just below the single-mode

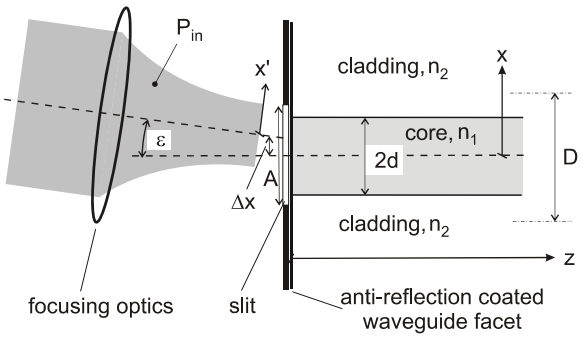

Fig. 1. Input radiation and geometry of slab waveguide

Proc. '6th Internat. Conf. on Space Optics', ESTEC, Noordwijk, The Netherlands, 27-30 June 2006 (ESA SP-621, June 2006)

cut-off frequency of V = π/2. The waveguide facet is assumed to carry an anti-reflection coating.

For the incident radiation we consider two cases: In the first (Sect. 4), a plane wave is focused onto the waveguide facet. In the focal plane it thus produces a field distribution proportional to

$$f(x') = \sin\frac{(\pi x'/x_N)}{x'}, \qquad (1)$$

i.e. a sinc function with the first zeros at x' = ± x_N. The transverse coordinate axes x' and x include the angle ε (see Fig. 1). The second case (Sect. 5), covers an incident Gaussian beam where the field distribution in the focal plane is proportional to

$$g(x') = \exp\left[-\left(\frac{x'}{w}\right)^2\right], \qquad (2)$$

with w being the beam radius. For both cases we will present here results for a field linearly polarized orthogonal to the plane of incidence, i.e. what is commonly known as TE polarization (transverse electric).

3. NUMERICAL METHOD

To analyze the field distribution in the waveguide we employ a rigorous electromagnetic numerical tool that is based on the Fourier modal method (FMM) [2]. FMM was originally developed in the field of grating theory. In recent years, however, a number of extensions added to the original code have made FMM a versatile and popular tool dealing effectively with a much wider variety of micro-optical elements. A characteristic of FMM is that it requires the structure under investigation to be divided into layers with respect to the propagation direction, e.g., the z-direction. The thickness of each layer is chosen such that the material parameters (e.g. the refractive index n) depend only on the transverse coordinates, i.e. x in the present case. Apart from the focusing optics, the structure shown in Fig. 1 can thus be modeled of three layers: A semi-infinite input layer represented by the uniform index distribution n = 1, a thin medium layer represented by the x-dependent index distribution of the slit, and a semi-infinite output layer represented by the x-dependent index distribution of the waveguide. The field distribution in each layer is described by a set of modes where each mode is represented mathematically by a Fourier series. The x-dependent material parameters are described by Fourier series as well. By adjusting the modes such that the field distributions fulfill Maxwell's boundary conditions at each layer interface, we obtain a system of linear equations that is solved numerically by matrix computation. The input field distribution behind the focusing optics of Fig. 1 is described by a set of plane waves which represent the modes of a uniform layer, and the output distribution is given by a set of guided and radiated modes which are specific to the waveguide structure. Finally, we note that the use of Fourier series makes the system periodic in x-direction. Despite this inherent periodicity, we are still able to analyze single elements such as waveguides by introducing thin absorbing perfectly matched layers along both sides of the calculation area parallel to the z direction [3]. These layers eliminate any significant field crosstalk between neighboring areas.

4. FOCUSED PLANE WAVE INPUT

4.1 Intensity Distribution

Fig. 2 to Fig. 6 present examples for the transition from the incident free-space radiation to the guided single-mode regime in the form of color coded intensity distributions for the case of a focused plane wave. The waveguide parameters are those specified in Sect. 2. The diagrams cover an area of 500 λ x 4000 λ of the waveguide (with unequal scale in the x- and z-direction) plus an area of 500 λ x 100 λ in front of the facet, thus showing also the converging input wavefront. The waveguide input facet (at z = 0) is to the left (vertical yellow line). The vertical color scale on the right indicates that the dynamic range of the visualization is some 40 dB. The core region with width 2d = 4.5 λ appears as the horizontal bar with high intensity, i.e. colored in red. The parameters chosen for Fig. 2 (distance between the first zeros of the field distribution $2x_N$ = 10.97 λ, perfect alignment) yield the highest possible coupling efficiency into the waveguide's fundamental mode, it may thus serve as a reference. The power not guided by the waveguide is radiated off in a number of "beams", the most intense one under an angle of approximately α = ±4.0°. Fig. 3 reveals that a mismatch of the input diameter $2x_N$ (by 64% in this specific case) increases the power fraction radiated off and reduces the angle α. Fig. 4 and Fig. 5 show that angular and transverse misalignment lead to drastically enlarged power radiation. While the asymmetric radiation of the unguided power for ε ≠ 0° in Fig. 4 was to be expected, the close-to-symmetric behavior for a transverse displacement (Δx ≠ 0) in Fig. 5 is quite surprising. Here the "main lobes" spread out more or less under the same angle as in the reference case of Fig. 2. Fig. 6 demonstrates the influence of a slit of width *A* arranged at the input facet. We chose a slit width equal to the distance between the first zeros

of the sinc function ($A = 2x_N$) and achieve an optical field with a remarkably low fraction of unguided power. However, with this arrangement about 10% of the incident power P_{in} are lost by the obscuration.

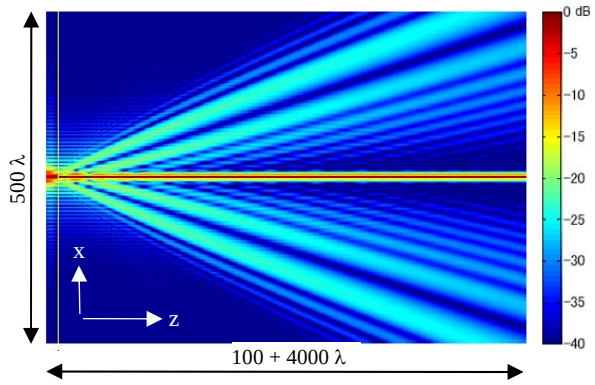

Fig. 2. Intensity distribution for focused plane wave (sinc function) for $2x_N = 10.97\ \lambda$, $\varepsilon = 0°$, $\Delta x = 0$, $A = \infty$.

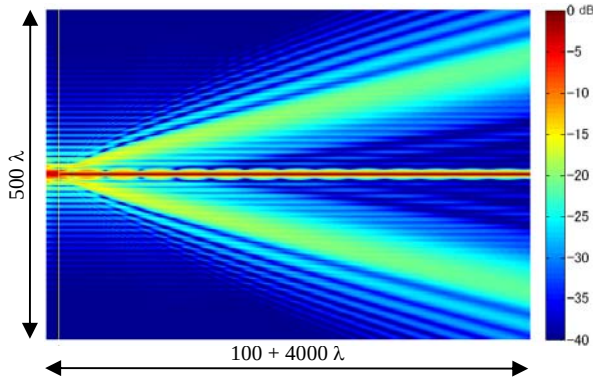

Fig. 3. As Fig. 2, but $2x_N = 18\ \lambda$.

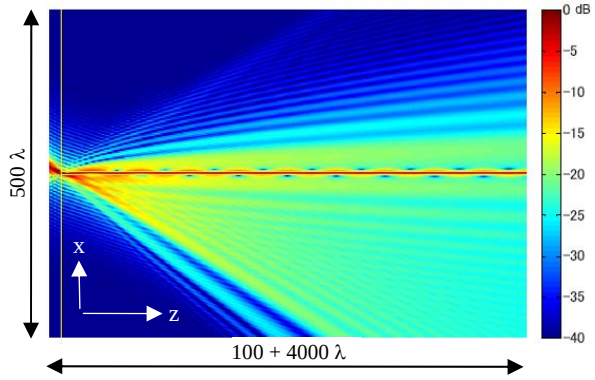

Fig. 4. As Fig. 2, but $\varepsilon = 5°$.

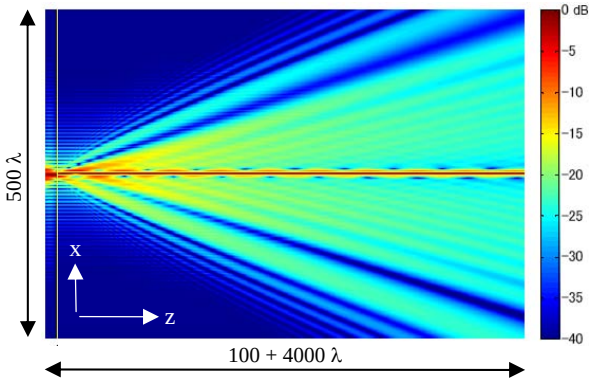

Fig. 5. As Fig. 2, but $\Delta x = 2.25\ \lambda$.

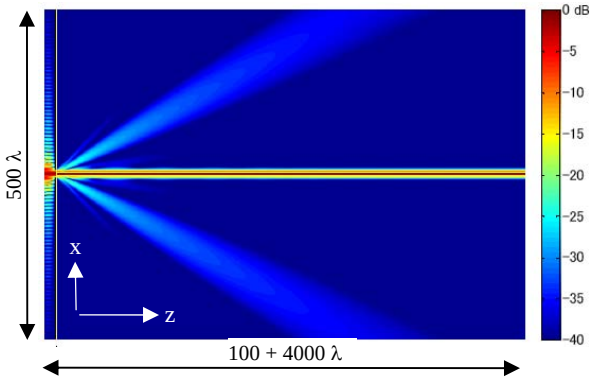

Fig. 6. As Fig. 2, but $A = 11\ \lambda$.

4.2 Near-Core Power

For the application of a single-mode waveguide as a modal filter it is paramount to know the formation of the – only – steady-state (i.e. guided) mode along the z-direction. To this end we calculate the fraction p(z) of power P contained within a width D (see Fig. 1) large enough to contain essentially all the fundamental mode's power. Our choice was $D = 18\ \lambda$. For the waveguide parameters chosen, this width contains 99.986% of the mode's power for $z \to \infty$. The quantity p(z) is normalized to the entire power illuminating the waveguide structure, P_{in},

$$p(z) = \frac{P_D(z)}{P_{in}}. \qquad (3)$$

The function p(z) hence reveals how the intensity distribution close to the core approaches the steady state of the fundamental mode. This allows estimating not only the required length of a modal filter. Also, for large z, p(z) approaches the value of the coupling efficiency into the fundamental mode (see next

section). Fig. 7 gives the function p(z) for the five examples presented in the previous section. The line corresponding to Fig. 6 shows a remarkable result: Not only does the near-core power reach a steady state within a comparably short distance from the input facet, but also does p(z) maintain a high level.

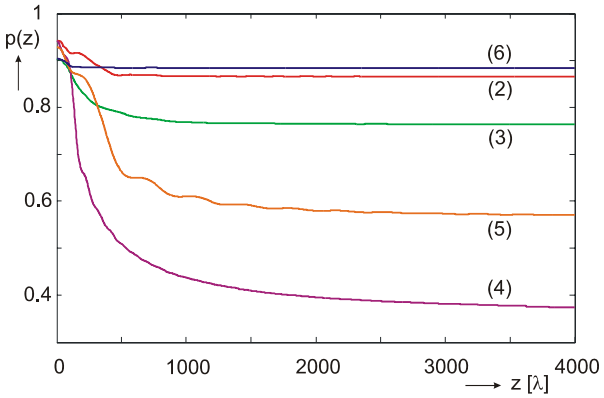

Fig. 7. Sinc input: Power fraction p(z) within a central area of width D = 18 λ (see Fig. 1). Labels (2) to (6) give the correspondence to the cases defined in Fig. 2 to Fig. 6, respectively.

4.3 Coupling Efficiency

We define the coupling efficiency η as the ratio of the power carried by the waveguide's single guided mode to the input power P_{in}. However, as the mode extends to infinity in x-direction, the numerical determination of η requires a slightly modified definition. We maintain sufficient accuracy when taking the power propagating within a width of, e.g., D = 18 λ in its limit for $z \to \infty$, designated $P_{D=18\lambda, z\to\infty}$,

$$\eta = \frac{P_{D=18\lambda,\, z\to\infty}}{P_{in}} . \qquad (4)$$

Table 1 summarizes η for the five cases addressed in Sect. 4.1. For the top four cases the numerically obtained values can easily be checked analytically. Full agreement was found. Note that positioning a slit of width $A = 2x_N$ at the facet of the waveguide in the otherwise optimal reference case entails a slightly higher value of coupling efficiency (η = 0.885) than that obtained for the reference case (η = 0.865).

Table 1. Examples of coupling efficiency η for focused plane wave input (sinc function), assuming a perfect anti-reflection coating on the waveguide facet.

η	$2x_N$ [λ]	ε [°]	Δx [λ]	A [λ]
0.865	10.97	0	0	∞
0.764	18	0	0	∞
0.376	10.97	5	0	∞
0.566	10.97	0	2.25	∞
0.885	10.97	0	0	11

5. FOCUSED GAUSSIAN BEAM INPUT

5.1 Intensity Distribution

Gaussian beams maintain their profile when focused (see Eq. (2)) and match the fundamental mode of most waveguides in general quite well. One could thus expect less power going into radiation modes, a more rapid development of the fundamental mode, and a higher coupling efficiency than for the case of a focused plane wave covered above. Fig. 8 to Fig. 11 present examples for such field transitions, as before in the form of color coded intensity distributions just before and after the waveguide facet. The waveguide parameters are those already given in Sect. 1. Fig. 8 covers the reference case (highest possible coupling efficiency) where the e^{-2}-beam diameter 2w has to be

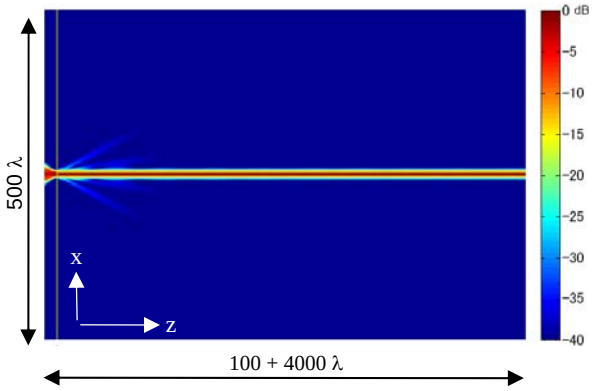

Fig. 8. Intensity distribution for focused Gaussian beam for 2w = 6.75 λ, ε = 0°, Δx = 0, $A = \infty$.

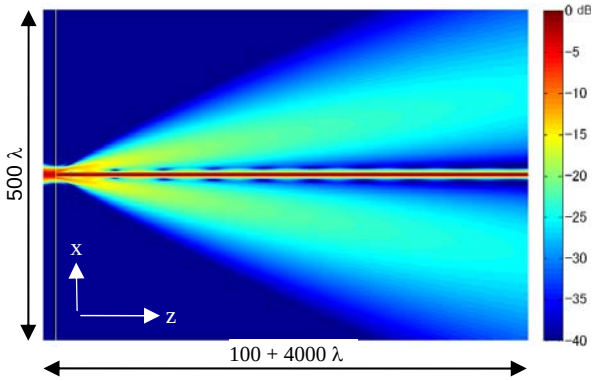

Fig. 9. As Fig. 8, but 2w =15 λ.

chosen as 2w = 6.75 λ. The (small amount of) power not guided is radiated off almost in two single "beams" under an angle of approximately α = ±5.7°. As before, the angular misalignment (Fig. 10) leads to an asymmetric distribution while the transverse misalignment does (almost) not (Fig. 11).

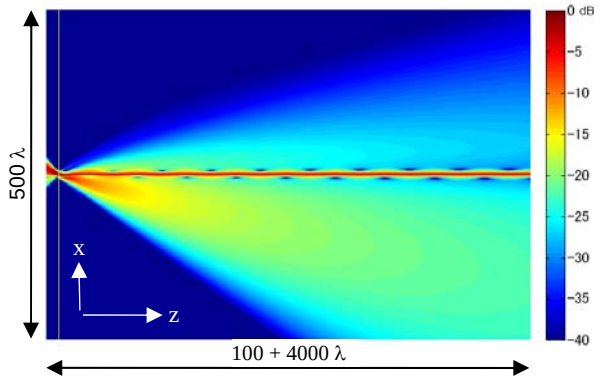

Fig. 10. As Fig. 8, but ε = 5°.

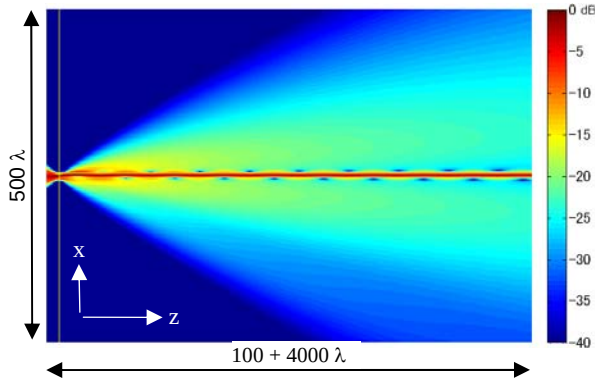

Fig. 11. As Fig. 8, but Δx = 2.25 λ.

5.2 Near-Core Power

The power p(z) propagating in and near the core, as defined in Sect. 4.2, was calculated also for Gaussian input beams. Fig. 12 gives the function p(z) for the four examples presented in the previous section.

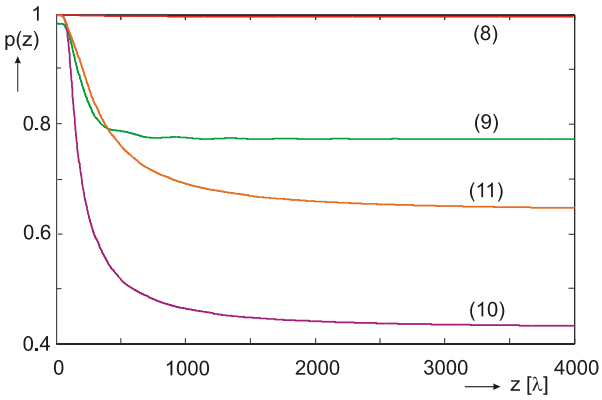

Fig. 12. Gaussian input: Power fraction p(z) within a central area of width D = 18 λ. Labels (8) to (11) give the correspondence to the cases defined in Fig. 8 to Fig. 11, respectively.

5.3 Coupling Efficiency

With the definition given by Eq. (4) the coupling efficiency η was calculated from the numerically obtained intensity distribution for the four cases of Gaussian input beams specified above (see Table 2). A value of η close to unity is obtained for optimized field match (2w = 6.75 λ). The penalty to pay for diameter mismatch is much less severe than for the sinc input field: For an input diameter of 2w = 15 λ corresponding to a relative mismatch of 122%, we still obtain a slightly higher efficiency than for the sinc case with a relative mismatch of 64%. Also the dependence of coupling efficiency on angular and transverse misalignment is less pronounced for the Gaussian input field. For all cases the numerically obtained values can easily be checked analytically. Again full agreement was found.

Table 2. Examples of coupling efficiency η for focused Gaussian beam. A perfect anti-reflection coating on the waveguide facet is assumed.

η	2w [λ]	ε [°]	Δx [λ]	A [λ]
0.996	6.75	0	0	∞
0.773	15.0	0	0	∞
0.431	6.75	5	0	∞
0.648	6.75	0	2.25	∞

6. SUMMARY AND OUTLOOK

The numerical method developed allows us to calculate the intensity distribution at the input end of optical waveguides, i.e. in the transition region from free-

space radiation to guided modes. We applied the technique to a dielectric step-index single-mode slab waveguide and made visible how the input power splits into radiation modes and into the waveguide's steady-state fundamental mode. Computing the power within and in close vicinity of the core as a function of the distance from the input facet, p(z), permits to assess the waveguide length necessary for obtaining a modal filter. As a by-product, the coupling efficiency into the fundamental mode is found. Although demonstrated here just for the two-dimensional case, the method already gives hints on how to design modal filters with high suppression of all but the guided modes. In the future we will apply the technique to more complicated waveguide structures modeling better what is found in reality, and also expand it to three-dimensional cases such as fibers.

7. REFERENCES

1. Wallner, O. et al., Minimum length of a single-mode fiber spatial filter, *JOSA-A*, Vol.19, 2445-2448, 2002.
2. Li L., New formulation of the Fourier modal method for crossed surface-relief gratings, *JOSA-A*, Vol. 14, 2758-2767, 1997.
3. Silberstein E. et al., Use of grating theories in integrated optics, *JOSA-A*, Vol. 18, 2865-2875, 2001.